Oral Oncology 149 (2024) 106678

Contents lists available at ScienceDirect

Oral Oncology

journal homepage: www.elsevier.com/locate/oraloncology

Molecular subtyping of head and neck cancer – Clinical applicability and correlations with morphological characteristics

Fabian Stögbauer [a,b,1], Raik Otto [c,1], Korinna Jöhrens [d], Ingeborg Tinhofer [e,f], Ulrich Keilholz [e,g,h], Christopher Poremba [i], Ulrich Keller [e,j,k,l], Ulf Leser [c], Wilko Weichert [a,b,m], Melanie Boxberg [a,b,h,m,2], Konrad Klinghammer [e,h,j,2,*]

[a] Technical University of Munich, Germany
[b] TUM School of Medicine and Health, Institute of General and Surgical Pathology, Germany
[c] Knowledge Management in Bioinformatics, Institute for Computer Science, Humboldt-Universität zu Berlin, Unter den Linden 6, 10099 Berlin, Germany
[d] Institute of Pathology, University Hospital Carl Gustav Carus, Fetscherstr. 74, 01307 Dresden, TU, Germany
[e] German Cancer Consortium (DKTK), Partner Site Berlin, Germany
[f] Department of Radiooncology and Radiotherapy, Charité-Universitätsmedizin Berlin, Germany
[g] Berlin Institute of Health, Berlin, Germany
[h] Charité Comprehensive Cancer Center, Berlin, Germany
[i] Pathologie München-Nord, Ernst-Platz-Str. 2, 80992 München, Deutschland
[j] Department of Hematology, Oncology and Cancer Immunology, Charité - Universitätsmedizin Berlin, Corporate Member of Freie Universität Berlin and Humboldt-Universität zu Berlin, Berlin, Germany
[k] Max-Delbrück-Center for Molecular Medicine, Berlin, Germany
[l] German Center for Translational Cancer Research (DKTK), DKFZ, Heidelberg, Germany
[m] German Cancer Consortium (DKTK), Partner Site Munich, Institute of Pathology, Munich, Germany

ARTICLE INFO

Keywords:
Head and neck cancer
Disease recurrence
NanoString
Tumor budding
Gene expression

ABSTRACT

Aim: We aimed to evaluate the applicability of a customized NanoString panel for molecular subtyping of recurrent or metastatic head and neck squamous cell carcinoma (R/M−HNSCC). Additionally, histological analyses were conducted, correlated with the molecular subtypes and tested for their prognostic value.
Material and Methods: We conducted molecular subtyping of R/M−HNSCC according to the molecular subtypes defined by Keck et al. For molecular analyses a 231 gene customized NanoString panel (the most accurately subtype defining genes, based on previous analyses) was applied to tumor samples from R/M−HNSCC patients that were treated in the CeFCiD trial (AIO/IAG-KHT trial 1108). A total of 130 samples from 95 patients were available for sequencing, of which 80 samples from 67 patients passed quality controls and were included in histological analyses. H&E stained slides were evaluated regarding distinct morphological patterns (e.g. tumor budding, nuclear size, stroma content).
Results: Determination of molecular subtypes led to classification of tumor samples as basal (n = 46, 45 %), inflamed/mesenchymal (n = 31, 30 %) and classical (n = 26, 25 %). Expression levels of *Amphiregulin* (*AREG*) were significantly higher for the basal and classical subtypes compared to the mesenchymal subtype. While molecular subtypes did not have an impact on survival, high levels of tumor budding were associated with poor outcomes. No correlation was found between molecular subtypes and histological characteristics.
Conclusions: Utilizing the 231-gene NanoString panel we were able to determine the molecular subtype of R/M−HNSCC samples by the use of FFPE material. The value to stratify for different treatment options remains to

Abbreviations: 5-FU, 5-fluorouracil; AJCC, American Joint Committee on Cancer; AREG, Amphiregulin; CT, computed tomography; ECOG, Eastern Cooperative Oncology Group; EGFR, epidermal growth factor receptor; HNSCC, head and neck squamous cell carcinoma; HPV, human papillomavirus; MCNS, minimal cell nest size; MRI, magnetic resonance imaging; PFS, progression-free interval; TB, tumor cell budding; WHO, World Health Organization.

* Corresponding author at: Department of Hematology, Oncology and Cancer Immunology, Charité - Universitätsmedizin Berlin, Corporate Member of Freie Universität Berlin and Humboldt-Universität zu Berlin, Hindenburgdamm 30, 12200 Berlin, Germany.
E-mail address: konrad.klinghammer@charite.de (K. Klinghammer).

[1] Shared first authorship.
[2] Shared last authorship.

https://doi.org/10.1016/j.oraloncology.2023.106678
Received 17 May 2023; Received in revised form 27 November 2023; Accepted 23 December 2023
Available online 13 January 2024

be explored in the future. The prognostic value of tumor budding was underscored in this clinically well annotated cohort.

Introduction

Squamous cell carcinomas of the head and neck (HNSCC) comprise one of the most prevalent malignancies in the western world [1]. In general, prognosis of recurrent or metastatic disease (R/M−HNSCC) remains poor and therapeutic options are limited to systemic treatment [2,3]. For more than a decade the standard of care in the palliative first-line setting was the EGFR monoclonal antibody cetuximab administered as an adjunct to cisplatin/carboplatin and 5-fluorouracil [4]. Recent clinical trials aimed to improve the outcome of R/M−HNSCC patients, amongst others the multicenter phase II Study CeFCiD, in which the efficacy of cetuximab, 5-flourouracil, and cisplatin with the same regimen adding docetaxel in R/M−HNSCC was tested [5]. The trial did not demonstrate a survival benefit from therapy intensification in first-line R/M HNSCC compared to standard therapy [5].

However, detailed survival analysis revealed that selected R/M−HNSCC patients potentially might benefit from therapy intensification and molecular tissue-based biomarkers might help to identify this subset of patients [5,6]. In particular, gene expression analyses are utilized to determine molecular profiles of various cancers which help to predict survival outcomes or treatment responses [7,8].

In several landmark studies including the TCGA, four gene expression subtypes in HNSCC were identified: basal, mesenchymal, atypical and classical [9,10]. Subsequently, significant differences of distinct subgroups concerning their treatment responses to e.g. cetuximab therapy were observed in preclinical models as well as in HNSCC patients [11,12]. Besides, increased expression of EGFR pathway members, especially *Amphiregulin* (*AREG*) and *Epiregulin* in the basal subtype, was correlated with treatment response to cetuximab in these models and in cell line studies [6,13].

As gene expression profiling by whole transcriptome sequencing is cost- and time-consuming and requires an extensive bioinformatic pipeline to determine the named molecular subgroups the applicability in the routine clinical setting is hampered [14,15]. Thus, the first aim of our study was to develop a more straightforward and easy to conduct approach to be possibly applied as a diagnostic procedure. Hence, a focused customized NanoString panel was created to assess the molecular subtypes of HNSCC and applied to the CeFCiD study population [5]. We developed this panel based on the classifier of Keck at al. since close correlation with morphologic characteristics, molecular processes, survival, and copy number changes supported a biologic and clinical basis for this validated approach. The NanoString approach was chosen as it allows for the robust and reliable analysis of formalin-fixed paraffin-embedded (FFPE) specimens [15].

Consequently, focusing on the CefCID study, the second aim was to elucidate morphomolecular biomarkers for patient prognosis in R/M−HNSCC patients. To this end, we focused on morphologic patterns which have been demonstrated to be of prognostic significance in the initial diagnostic setting in treatment-naïve patients: tumor budding (TB), proliferation (mitotic activity), stroma content, lymphocytic infiltrate and the molecular subtypes determined by the NanoString panel [16–22].

TB is supposed to be the morphologic correlate of aggressive tumors leading to lymph node and distant metastases [23]. Its prognostic significance could be shown for many tumor entities including head and neck cancer [24–26]. While in previous studies in head and neck cancers, primary tumors of therapy-naïve patients were analyzed, information on the predictive and prognostic impact of TB in the R/M−HNSCC are to the best of our knowledge up to date not available [27].

We hypothesized a correlation between molecular subtypes and histopathological patterns demonstrating the informative value of our customized 231-gene NanoString panel in clinical practice. Furthermore, we aimed to test the prognostic significance of TB and other potential morphologic biomarkers in a R/M−HNSCC cohort and mutual correlations of morphologic and molecular parameters.

Materials and methods

Study design

The CeFCiD trial was designed as a prospective, open-label, randomized, multicenter phase II study at 15 centers in Germany evaluating treatment intensification by the addition of docetaxel to platinum, 5-FU and cetuximab [5]. Patient consent for molecular analyses and translational research was given at study entry as part of the informed consent to trial enrollment. Participating trial centers were asked to provide FFPE tissue from enrolled patients in 2016. All analyses were conducted in accordance with the Declaration of Helsinki.

The CeFCiD trial included 180 patients for first line treatment of R/M−HNSCC. Detailed patient characteristics, study protocol data and inclusion and exclusion criteria were described previously [5]. The primary endpoint of the study was progression-free survival (PFS), which was determined as the time between study entry and the first radiologic confirmation of disease progress or death from any cause.

Histological analyses

Histological analyses were conducted on digitized H&E stained slides of FFPE material. Slides were scanned on a slide scanner (Aperio AT2, Leica Biosystems GmbH, Nussloch, Germany) and evaluated on a standard monitor (Fujitsu B24T-7, Fujitsu Limited, Tokyo, Japan, resolution 1920 x 1080) utilizing Aperio ImageScope x64 (version 12.4.0.7018; Leica Biosystems GmbH, Nussloch, Germany). One digitized high-power field (HPF) comprised 97 464 μm^2 which corresponded to a field diameter of 0.35 mm in light microscopy. The slides were analyzed independently by two experienced pathologists (FS, MB) who were blinded to clinicopathological parameters (Table 1). Cases with different results between both raters were reevaluated and discussed until a consensus was reached.

Histological classification of tumors into conventional and basaloid was conducted according to the current WHO classification of tumors of the head and neck [28]. Subsequently, conventional HNSCC were subtyped into keratinizing and non-keratinizing cases as previously described [17]. Histopathologic grading (G1/G2/G3) was performed according to the WHO classification [28]. The assessment of TB was conducted as previously described [17]. In short, TB was defined as the detachment of four or less tumor cells from the main tumor mass which infiltrated the adjacent stroma. First, slides were scanned at low-power magnification to identify the area with highest budding activity (hotspot area) and subsequently this area was analyzed at high-power magnification in one HPF.

According to previous publications, minimal cell nest size (MCNS) was defined as single tumor cells or the minimal number of cohesive tumor cells, respectively, which were detached from the main tumor mass and invaded the adjacent stroma [17]. For the assessment of mitoses a tumor area was chosen in analogy to TB evaluation and the number of tumor cell mitoses was recorded for one HPF. Stroma content, necrosis and lymphocytic infiltrate were evaluated at low-power magnification within the borders of the invasive tumor. Here, the area which was covered by the invasive carcinoma and the areas which were covered by stroma/necrosis/lymphocytes were estimated.

Subsequently, the ratio of areas covered by stroma/necrosis/lymphocytes and areas covered by invasive carcinoma was calculated as a percentage. For the estimation of stroma content and lymphocytic infiltrate, necrotic areas were excluded from the assessment. The nuclear size was determined as the average multiple of the nuclear size of tumor cells compared to adjacent lymphocytes [16]. Perineural invasion was defined as previously described [22]. The presence of tumor formations in lymphatic vessel lumina was defined as lymphovascular invasion.

RNA extraction

RNA extraction and NanoString analyses were conducted as previously described [30]. In short, H&E stained slides of HNSCC cases were examined to identify tumor regions and to estimate tumor cell content. Tumor regions were annotated by a pathologist (MB) and subsequently, microdissection for RNA extraction was conducted from 3 µm thick sections. Only areas with a minimal tumor cell content of 20 % (median 65 %) were used. RNA was then extracted according to manufacturer's instructions on a Maxwell extraction system (Promega, Madison, WI) and quantified by Qubit (Thermo Fisher Scientific, Waltham, MA).

NanoString panel design & analyses

Gene selection for the panel design was based on their expression values in previous analysis of molecular subtypes [31]. All genes included in the panel are listed in Supplemental table 1. Genes with the strongest statistical correlation to a particular subtype were chosen. Panel validation was done employing previously analyzed samples with an assigned molecular subtype [6]. For mRNA expression analyses, 400 ng (concentration 100 ng/µl) isolated RNA per sample were hybridized on a nCounter Analysis System using a customized NanoString panel consisting of 231 genes according to manufacturer's instructions (NanoString Technologies, Seattle, WA). The nCounter System and the nSolver Analysis software were applied for quantification and extraction of absolute read counts (NanoString Technologies, Seattle, WA). Additional in-silico quality control and follow-up analyses of the NanoString data were conducted using the Bioconductor package 'NanoStringNorm' [32]. Molecular data are available on Gene Expression Omnibus under GSE212070.

Molecular subtype classification

Samples were assigned a molecular subtype class based on a centroid classification approach. The centroid consisted of the subtype-defining genes chosen from the previously published centroid by Keck et al. [31]. For molecular subtyping the three "supergroups" according to the classification by Keck et al. were used: basal, classical and inflamed/mesenchymal. A successful subtype assignment was obtained by a stepwise approach for each sample to: *step A)* pass the bioinformatic quality control assurance; *step B)* subtype classification for samples quantified by a p-value lower than 0.05 (under exclusion of samples with $p \geq 0.05$); *step C)* compare transcriptomic similarity between subtype assignment and bioinformatic clustering of each sample - resulting in inclusion of samples with overlap between assigned subtypes and corresponding bioinformatic clustering. Hence, samples which were assigned a subtype "X" but which were located in cluster "Y" were assumed to be wrongly assigned. Those samples (n = 23) were excluded from further analysis.

Dataset normalization was conducted with the 'NanoStringNorm' R-package, version 1.2.1 [32]. The 'stringR' and 'ggplot2' packages in conjunction with the 'pheatmap' R-package (RRID:SCR_016418) were utilized for visualization and string manipulation [33,34]. For differential expression analyses, the 'LIMMA' R-package was utilized [35,36]. For computational analysis R (version 4.1.3) [37] and SPSS v25 (International Business Machines Corporation (IBM), Armonk, NY) were used.

Table 1
Clinicopathological data of the CeFCiD cohort (n = 57 patients with complete follow-up data, histopathological and transcriptomic data).

	Whole cohort		Treatment arm A		Treatment arm B		Basal subtype		Classical subtype		Inflamed/mesenchymal subtype	
	n	%	n	%	n	%	n	%	n	%	n	%
Age (years; median/IQR)	60 (IQR 11)		58 (IQR 9)		61.5 (IQR 7.8)		57 (IQR 7)		59 (IQR 8.8)		63.5 (IQR 7)	
Sex												
male	51	89.5	26	83.9	25	96.2	21	84	15	93.8	15	93.8
female	6	10.5	5	16.1	1	3.8	4	16	1	6.2	1	6.2
Tumor stage												
3	6	10.5	5	16.1	1	3.8	3	12	2	12.5	1	6.2
4	51	89.5	26	83.9	25	96.2	22	88	14	87.5	15	93.8
Grading												
1	1	1.8	1	3.2	0	0	1	4	0	0	0	0
2	40	70.2	23	74.2	17	65.4	19	76	11	68.8	10	62.5
3	16	28.1	7	22.6	9	34.6	5	20	5	31.2	6	37.5
Lymphovascular invasion												
absent	47	82.5	26	83.9	21	80.8	21	84	12	75	14	87.5
present	10	17.5	5	16.1	5	19.2	4	16	4	25	2	12.5
Perineural invasion												
absent	54	94.7	29	93.5	25	96.2	23	92	16	100	15	93.8
present	3	5.3	2	6.5	1	3.8	2	8	0	0	1	6.2
Localization												
Hypopharynx	13	22.8	8	25.8	5	19.2	6	24	3	18.8	4	25
Larynx	11	19.3	6	19.4	5	19.2	7	28	1	6.2	3	18.8
Oral cavity	8	14.0	5	16.1	3	11.5	4	16	3	18.8	1	6.2
Oropharynx	14	24.6	4	12.9	10	38.5	3	12	6	37.5	5	31.2
Tongue	7	12.3	5	16.1	2	7.7	4	16	1	6.2	2	12.5
Tonsil	4	7.0	3	9.7	1	3.8	1	4	2	12.5	1	6.2
Histotype												
basaloid	4	7.0			4	15.4	0	0	1	6.2	3	18.8
conventional (keratinizing)	29	50.9	20	64.5	9	34.6	18	72	7	43.8	4	25
conventional (non-keratinizing)	24	42.1	11	35.5	13	50	7	28	8	50	9	56.2
Keratinization												
absent	26	45.6	12	38.7	14	53.8	8	32	9	56.2	9	56.2
present	31	54.4	19	61.3	12	46.2	17	68	7	43.8	7	43.8

Statistical analyses

Comparisons between nominal and ordinal-scaled variables were calculated with Fisher's exact test. For continuous data, the Mann-Whitney-U-Test was applied. Associations between variables were calculated with Pearson's Product-Moment Correlation. The Kaplan-Meier method was used to estimate overall and progression-free survival intervals and comparisons between groups were calculated with the Log-Rank-test. All tests were conducted two-sided and p-values < 0.05 were considered statistically significant.

Cutoff identification

Patient stratification according to the histological characteristics (TB, MCNS, mitotic activity, stroma content, necrosis, lymphocytic infiltrate, nuclear size) was conducted utilizing "Cutoff Finder" [29]. For each parameter patients were stratified into two groups according to the most significant results of a Log-Rank test calculated for PFS starting at the date of study entry. For lymphovascular invasion, perineural invasion and keratinization cases were stratified with regards to the absence or presence of the corresponding characteristic.

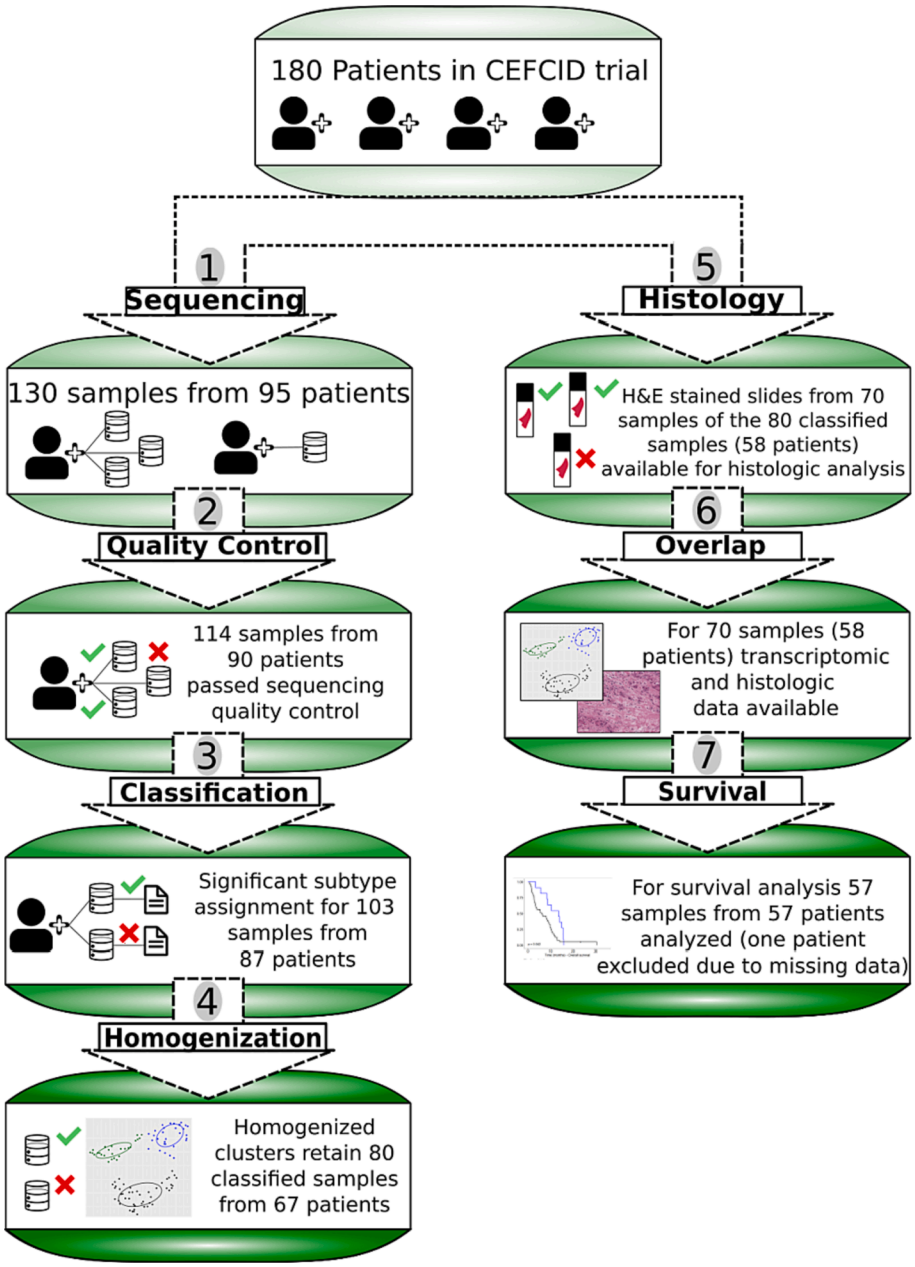

Figure 1. In the CEFCID trial 180 patients were randomized, which is the Intention-To-Treat population. Sequencing raw data for 130 samples from 95 patients was available for analyses (1). 114 samples from 90 patients passed the sequencing data quality control (2). We could assign a molecular subtype to 103 samples from 87 patients with statistical significance (p-value < 0.05; (3)). We homogenized the subtype clusters by discarded samples whose subtype did not match their cluster's subtype which left 80 samples from 67 patients for down-stream analyses (4). In parallel, histologic slides in adequate quality were available from 70 (of the 80 samples selected in (4)) from 58 patients (5). Samples/patients completely overlapped between molecular and morphologic analysis (6). For subsequent survival analysis, we included all patients with complete molecular and morphologic data and complete follow-up data - which rendered 57 patients available for survival calculations. One sample/patient with complete morphomolecular data was lost due to incomplete survival data (7). Of note, as recommended in literature, morphomolecular data obtained from the most recent sample was included. Thus, survival analyses are based on 57 samples from 57 patients (7)).

Results

Molecular subtypes of R/M−HNSCC

FFPE material – obtained at different dates during the course of the disease – was available for 130 samples from 95 patients of the CeFCiD cohort. 114 (88 %) passed the sequencing data quality control (RNA-degradation, tumor purity). We could assign a statistically significant molecular subtype (p-value < 0.05) via the Keck et al. centroid classifier to 103 (90 %) samples [31]. We excluded 23 samples that were located in a cluster that differed from their subtype (details are given in the materials and methods section above), with 80 (78 %) samples from 67 patients remaining for down-stream analyses (Figure 1).

From eight patients (11.9 %) more than one sample was obtained and included in transcriptomic analysis (Supplemental Table 2). In contrast, for survival analysis (see below) only the most recently obtained sample per patient was utilized as recommended by Weber et al. [38].

Most samples were obtained from the primary tumor (n = 37, 46 %, percentages relate to the 80 remaining samples) followed by samples obtained from recurrences (n = 22, 28 %) and samples without according information (n = 19, 24 %). Two samples (3 %) were obtained from lymph node metastases. Detailed clinicopathological information about the study cohort is shown in Table 1 and Supplemental table 2.

For survival analysis only patients for whom complete metadata regarding molecular subtypes, histomorphology and follow-up were available were included. Hence, 57 of 67 patients remained for survival analysis (Figure 1).

Utilizing our customized 231 gene NanoString panel, most samples were assigned to the basal subtype (n = 46, 45 %) followed by the inflamed/mesenchymal (n = 31, 30 %) and classical (n = 26, 25 %) subtypes (Figure 1). Down-stream analyses such as survival and histological correlations were only run on the 80 (78 %) classified samples from 67 patients whose subtype matched that of the subtype cluster they were located in, see Figure 2. Molecular subtyping did not yield prognostic significance regarding survival for none of the outcome variables ($p > 0.05$ each).

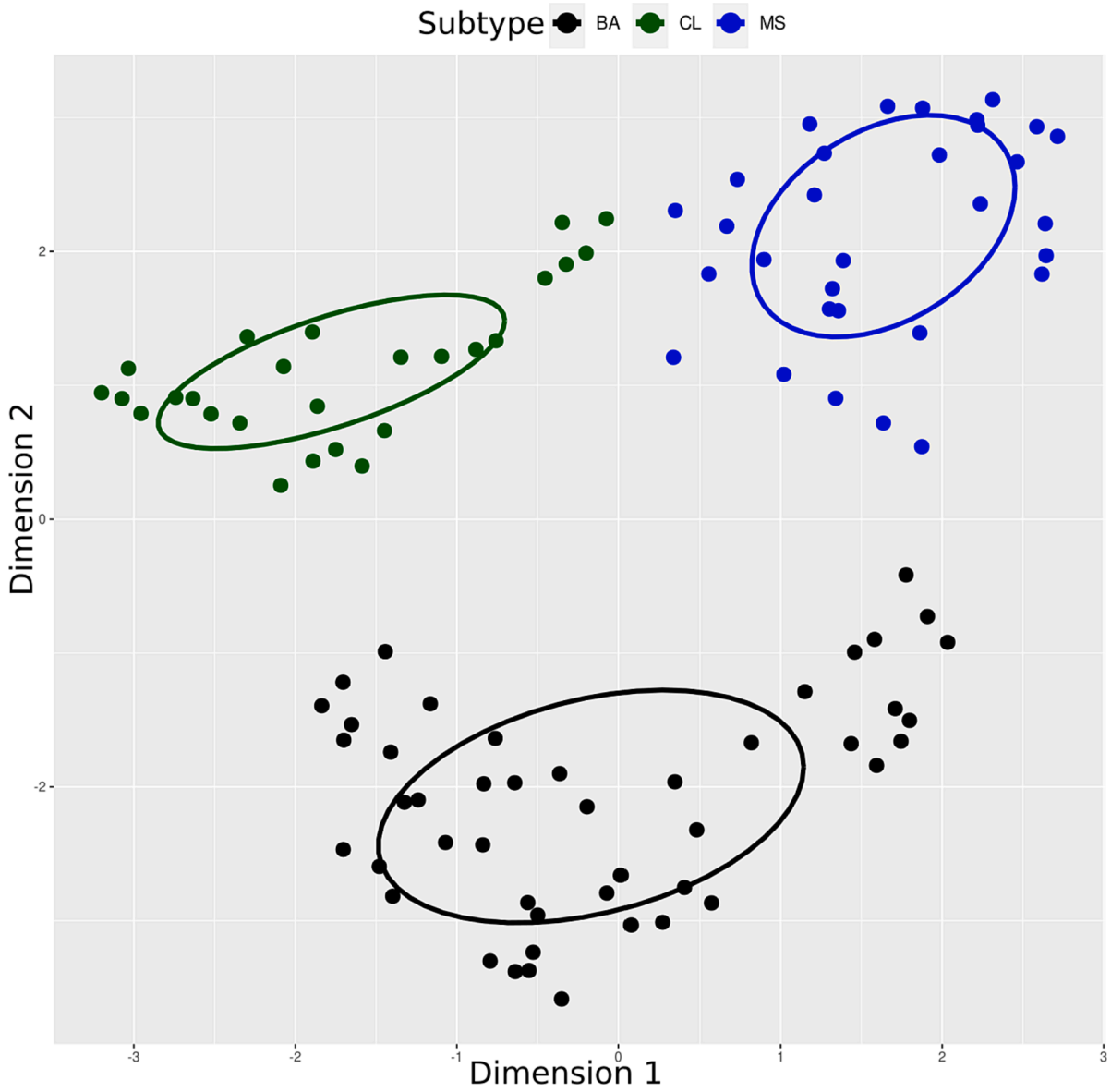

Figure 2. UMAP of the samples annotated by their molecular subtype. A projection of the high-dimensional transcriptomic data onto a two-dimensional plane visualizes that molecular clusters are identifiable and distinct from each other. A sample's position indicates its relative similarity of its transcriptome to all 103 samples with significant p-values based on the gene expression.

Gene expression of EGFR pathway members differ between molecular subgroups

Significant differences between subtypes with respect to gene expression levels of *AREG* were detected (Figure 3), revealing that the basal subtype showed a positive log fold change of 1.6 ($p < 0.001$) relative to the classical subtype and of 2.4 ($p < 0.001$) relative to the inflamed/mesenchymal subtype. Furthermore, significantly higher expression levels of *AREG* could be determined for the classical subtype compared to the inflamed/mesenchymal subtype (log fold change 0.8, $p = 0.01$).

For the *EGFR* gene, a significant differential expression was observed between the basal and inflamed/mesenchymal subtype (log fold change 0.8, $p = 0.027$).

Patient stratification using histological parameters

Regarding grading, 1 tumor was graded as G1, 49 tumors as G2 and 20 tumors as G3 (no information for $n = 10$ cases). As only one tumor was graded as G1, G1 and G2 tumors were combined. For 10 of the 80 (12.5 %) samples which could be assigned a molecular subtype, while passing quality control, the quality of H&E staining was not high enough to allow a detailed analysis of morphological patterns. Exemplary illustrations of the histological parameters analyzed are shown in Supplemental figure 1.

Metrics (median, interquartile range, mean, standard deviation, minimum, maximum) for the continuous histological parameters are shown in Supplemental table 3.

Patient stratification based on the cutoffs identified by "Cutoff Finder" resulted in 2-tiered classification schemes for all histological parameters. The cutoffs and the corresponding distribution of samples are shown in Supplemental table 4.

Survival analyses reveal TB as potential prognostic parameter

Survival analyses were conducted after patient stratification with regards to the cutoffs identified by "Cutoff Finder". Log-Rank tests and univariate Cox models were calculated for PFS and overall survival (OS) starting from the date of randomization (with PFS starting from the date of randomization representing the primary endpoint of the initial CeF-CiD trial) as well as PFS and OS starting from the date of initial diagnosis.

Among the histological parameters TB demonstrated prognostic significance. Here, cases with high TB showed shorter survival rates compared to cases with low TB for OS starting from the date of study entry (median 6.2 months vs. 13.6 months; $p = 0.042$, Figure 4). Moreover, a low mitotic count (median 5.4 months vs. 8.9 months; $p = 0.009$) and a big nuclear size (median 3.4 months vs. 5.6 months; $p = 0.038$) were associated with inferior survival rates for PFS starting from the date of randomisation.

Results of the Log-Rank tests along with the hazard ratios tests for the histological parameters are summarized in Table 3.

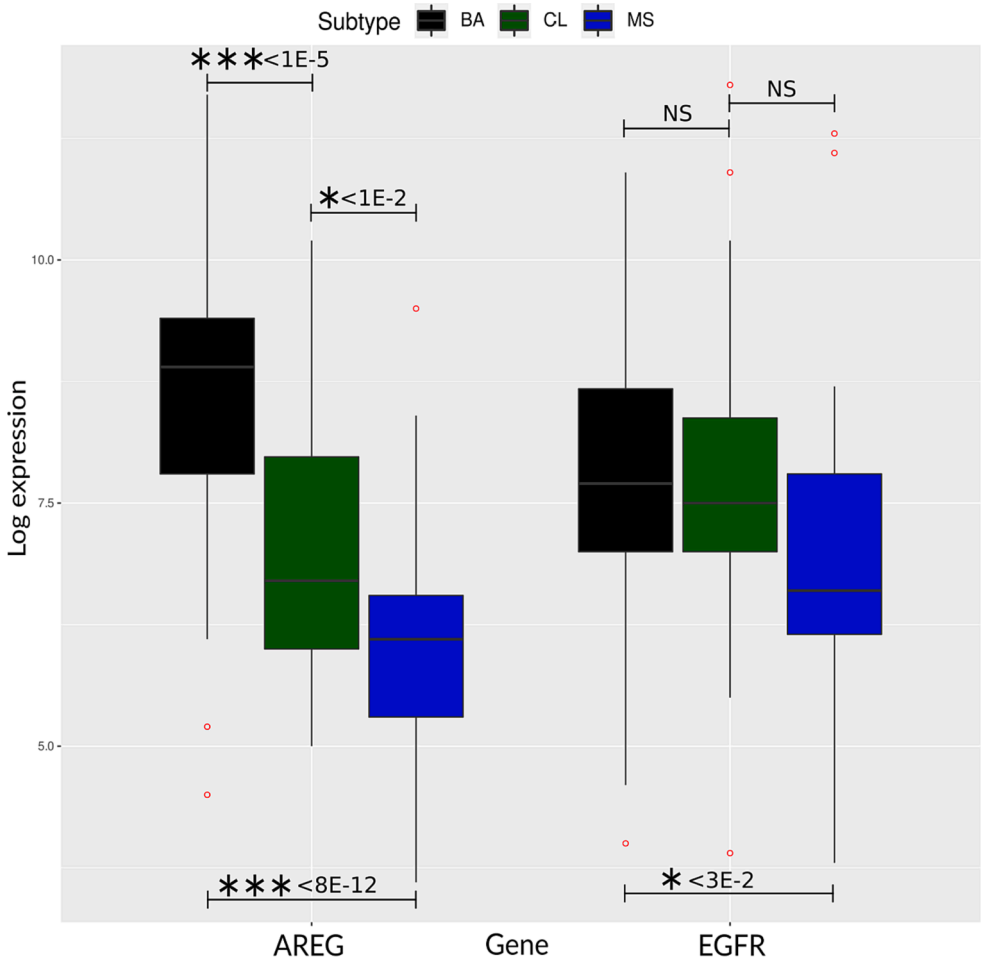

Figure 3. *AREG* and *EGFR* gene expression for each subgroup. A significantly higher expression of *AREG* could be detected in the basal and classical subtype compared to the mesenchymal subtype. The *EGFR* gene was significantly higher expressed in the samples with a basal subtype classification relative to samples classified as having a mesenchymal subtype (BA: basal subtype, CL: classical subtype, MS: mesenchymal subtype).

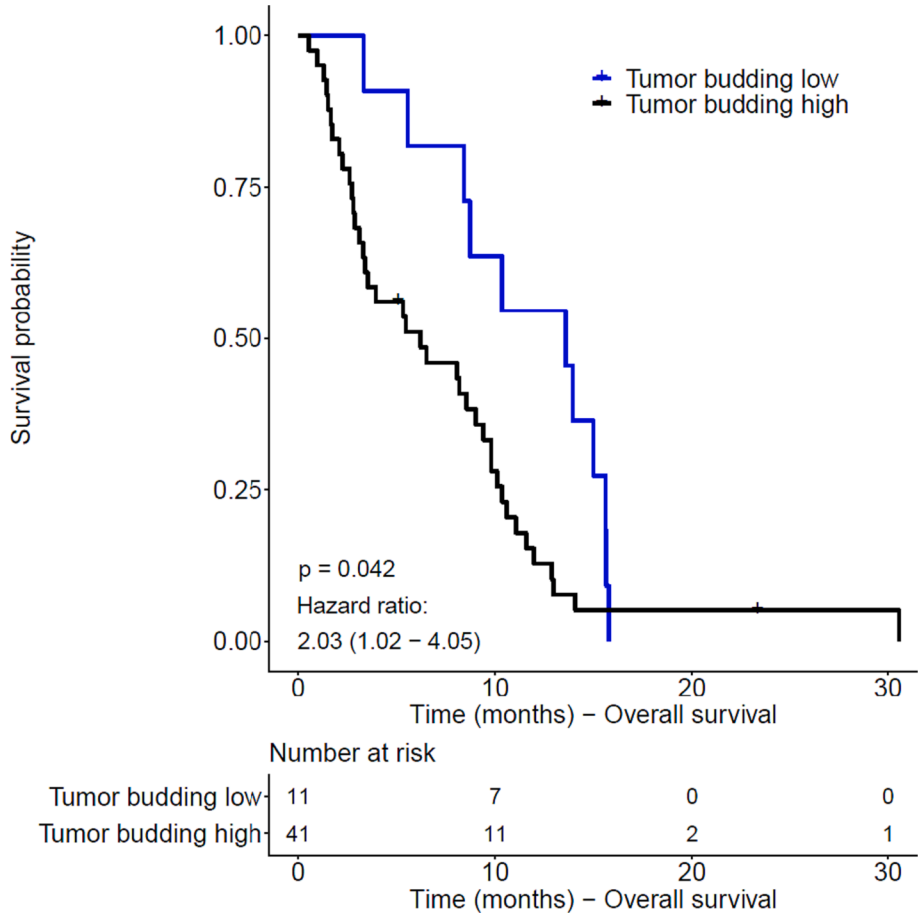

Figure 4. Kaplan-Meier plot for overall survival (starting from the date of randomisation) after stratification for tumor cell budding.

Clinicopathological and histological correlations with molecular subtypes

Pearson's Product-Moment Correlation was calculated for the histological parameters (Supplemental figure 2). Here, dense inflammatory infiltrate was correlated with a bigger cell nest size ($r = 0.26$, $p = 0.03$) whereas bigger nuclear sizes were associated with smaller MCNS ($r = -0.30$, $p = 0.01$). High TB was associated with smaller cell nest sizes ($r = -0.34$, $p = 0.005$), less inflammation ($r = -0.26$, $p = 0.03$) and higher amounts of necrosis ($r = 0.26$, $p = 0.03$).

Considering the classification of samples with respect to the cutoffs identified, a high budding activity was associated with a higher number of G3 tumors (35.1 % vs. 0 %) and a lower number of G1/G2 tumors (64.9 % vs. 100 %; $p = 0.014$). Furthermore, tumors with a high amount of necrosis were more often basaloid (20.7 % vs. 0 %) and conventional (keratinizing) (51.7 % vs. 46.3 %) and less often conventional (non-keratinizing) (27.6 % vs. 53.7 %; $p = 0.002$). Similarly, tumors with a high amount of necrosis were associated with perineural invasion (17.2 % vs. 0 %; $p = 0.010$). Additionally, tumors with high-grade inflammation showed more often G1/G2 differentiation (81.2 % vs. 50.0 %; $p = 0.011$). Correlations for clinical and histological parameters are shown in detail in Table 2 and Supplemental table 5.

Discussion

Prognosis of most patients with R/M−HNSCC is unfavorable and up to date, established biomarkers to predict treatment responses in the R/M−HNSCC setting are lacking [39]. However, molecular subtypes based on gene expression patterns have been defined resembling the biological nature of the disease with potential prognostic and predictive implications. Furthermore, histological parameters might help in prognostic classification of patients and therefore in planning of follow-up procedures.

Different molecular classifiers for head and neck cancer have been published with largely overlapping signatures. The classifier by Keck at al. demonstrated three biological distinct molecular subgroups with two additional subgroups of HPV positive tumors in classical or mesenchymal/inflamed subtype. The group validated their signatures on a large independent cohort which underlined the feasibility of their classifier. We therefore based our analyses on the work of Keck et al. Utilizing our highly compact NanoString panel, we were able to determine the molecular subtype of R/M−HNSCC in a vast majority of cases showing the applicability of this panel in clinical practice. To our knowledge this is the first study determining molecular subtypes of R/M−HNSCC based on a NanoString approach which in our experience is fast, cost-effective and sufficiently performant on FFPE material [14,15]. The applicability and robustness of the NanoString nCounter platform has been shown previously, enabling researchers to conduct gene expression analyses even for samples with low RNA quality (e.g. FFPE material) [15]. In conclusion, the NanoString approach shows advantages compared to whole transcriptome analyses rendering it applicable for clinical practice. On the other hand, the limited number of genes evaluated on such a panel based approach in contrast to RNA sequencing bears the potential of missing gene expression profiles which might become of interest in the future. A further limitation of the small panel we used became obvious when we excluded 23 samples from the entire cohort due to the fact that bioinformatic clustering did not align with transcriptomic similarity. By choosing this rigorous approach we intended to minimize the chance of misclassification.

At the gene expression level, *Amphiregulin* (*AREG*) constitutes one of the ligands of EGFR [40]. For R/M−HNSCC it could be shown that

Table 2
Clinical and histological correlations of the CeFCiD cohort.

	Number of samples with available data	Budding		
		low	high	p
Age (median; IQR)	70	58 (11)	61 (8)	0.607
Sex				
male	64	11 (84.6)	53 (93.0)	0.308
female	6	2 (15.4)	4 (7.0)	
Tumor stage				
3	10	0 (0.0)	10 (17.5)	0.190
4	60	13 (100.0)	47 (82.5)	
Grading				
G1/G2	50	13 (100.0)	37 (64.9)	**0.014**
G3	20	0 (0.0)	20 (35.1)	
Histotype				
basaloid	6	0 (0.0)	6 (10.5)	0.118
conventional (keratinizing)	34	4 (30.8)	30 (52.6)	
conventional (non-keratinizing)	30	9 (69.2)	21 (36.8)	
Localization				
Hypopharynx	17	2 (15.4)	15 (26.3)	0.882
Larynx	14	2 (15.4)	12 (21.1)	
Oral cavity	10	2 (15.4)	8 (14.0)	
Oropharynx	14	3 (23.1)	11 (19.3)	
Tongue	8	2 (15.4)	6 (10.5)	
Tonsil	7	2 (15.4)	5 (8.8)	
Lymphangiosis				
absent	56	11 (84.6)	45 (78.9)	>0.999
present	14	2 (15.4)	12 (21.1)	
Perineural invasion				
absent	65	13 (100.0)	52 (91.2)	0.576
present	5	0 (0.0)	5 (8.8)	
Subtype				
basal	30	4 (30.8)	26 (45.6)	0.282
classical	19	6 (46.2)	13 (22.8)	
mesenchymal/ inflamed	21	3 (23.1)	18 (31.6)	

higher expression levels of *AREG* expression predicted response to cetuximab monotherapy [41]. In our study we could detect significantly higher gene expression levels for *AREG* in the basal and in the classical subtype compared to the mesenchymal/inflamed subtype. Therefore, not only could we demonstrate the applicability of our NanoString panel in assigning the molecular subtype of R/M−HNSCC but also validate the high expression of *AREG* in the basal subtype which has been associated with treatment response to cetuximab therapy in preclinical models [6]. Furthermore, for patients with metastatic colorectal cancer it could be shown that high levels of *AREG* expression predict disease control for cetuximab monotherapy [42]. However, the prognostic and predictive implications of different *AREG* gene expression levels in the molecular subtypes of HNSCC have to be addressed in prospective clinical studies analyzing larger patient cohorts.

After patient stratification with regards to the molecular subtype we did not have any power to detect differences in PFS or OS. This might be explained by the limited effect sizes or the small cohort sizes of the molecular subgroups and the fact that both treatment arms within the CeFCiD trial contained the EGFR antibody [38,43,44]. An increase in the cohort size in studies tailored to this question might help to detect survival differences for each molecular subgroup.

Analyzing the histological characteristics of the study cohort, prognostic significance with poor outcomes could be shown for high TB for OS, and a low mitotic count and a big nuclear size for PFS. Especially the evaluation of TB might help in the prognostic stratification of R/M−HNSCC patients considering that high TB has already been shown to be associated with adverse outcomes in previous publications which included treatment-naïve patients [17,45]. To the best of our knowledge, this study is the first to demonstrate a significant adverse prognostic impact of TB in the R/M−HNSCC setting potentially allowing a more personalized follow-up care for patients with R/M−HNSCC [46]. However, studies on larger cohorts are needed to validate the prognostic relevance of TB in R/M−HNSCC patients.

Tumor budding is considered to be the morphological correlate of epithelial-mesenchymal transition and therefore, one could expect higher TB in mesenchymal/inflamed tumors [26,47]. However, we could not detect an association between the molecular subtypes and TB. Interestingly, we could observe a negative correlation between TB and inflammation, which might contribute to the inferior survival outcomes of patients with high TB compared to patients with low TB – a correlation which has been observed in previous studies in oral HNSCC [48]. Therefore, the aggressive biological behavior of cases with high TB leading to lymph node and distant metastases might partially be accompanied and supported by the lower inflammatory infiltrate detected in these tumors facilitating immune escape mechanisms [25,49,50]. Especially in the light of choosing between immunotherapy and chemotherapy in the R/M setting this factor might be of high relevance for treatment stratification. Thus, attempts to modulate the immune response in tumors with high TB should be examined in future studies [51]. As expected, G1 and G2 tumors showed lower TB scores but showed a higher inflammatory infiltrate. Similarly, the association between grading and the immune infiltrate might be therapeutically exploited in the future.

There are some limitations of our study that have to be considered. Applying the NanoString panel we were able to assign the molecular subtype of R/M−HNSCC cases. However, there might be targeted therapies for which therapy prediction of efficacy might be based on the gene expression profiles of genes that are not included in the 231 gene panel and therefore require additional molecular analyses. Furthermore, for histological analyses only H&E stained slides were available. Hence, no additional studies (e.g. immunohistochemical analyses of immune cell subpopulations) could be conducted. The cohort size was limited which did not allow a detailed analysis considering both treatment arms separately. In addition, study enrollment was conducted irrespective of HPV status which was therefore not available. Thus, the patients could not be stratified according to this parameter and mutual correlations of the HPV status with histological and molecular data could not be determined.

Conclusion

We were able to conduct molecular subtyping of R/M−HNSCC samples based on a customized NanoString approach. Especially in the light of evolving concepts of therapy stratification based on tumor biology in head and neck cancer, the easy-to-use approach of NanoString analysis on FFPE stored tissue proves the feasibility to determine the molecular subtype as well as a differential expression of selected potentially predictive genes of R/M−HNSCC. Furthermore, we conducted a comprehensive analysis of tissue-based biomarkers in the prospective phase II study CeFCiD. Patient prognosis differed based on the histopathological parameter tumor budding (TB), which therefore might be a promising parameter for prognostic stratification of R/M−HNSCC patients underlining the major future importance of morphology.

Table 3
Hazard ratios are reported which were calculated for each histological variable and the molecular subtype. Additionally, corresponding p-values are shown.

	Progression free survival from randomization	p	Overall survival from randomization	p	Progression free survival from diagnosis	p	Overall survival from diagnosis	p
Subtype (basal = 1)		0.269		0.184		0.785		0.758
classical	1.24 (0.60—2.56)		0.56 (0.27—1.14)		1.22 (0.60—2.47)		0.77 (0.38—1.56)	
mesenchymal/inflamed	0.66 (0.34—1.30)		0.62 (0.32—1.21)		1.22 (0.62—2.39)		0.98 (0.50—1.91)	
Histotype (basaloid = 1)		0.926		0.784		0.788		0.323
keratinizing	1.16 (0.35—3.88)		1.24 (0.37—4.13)		0.85 (0.26—2.85)		0.60 (0.18—2.02)	
non-keratinizing	1.05 (0.31—3.56)		1.01 (0.30—3.46)		0.72 (0.21—2.49)		0.43 (0.12—1.50)	
Grading (G1/G2 = 1)		0.655		0.782		0.775		0.730
G3	1.16 (0.61—2.20)		0.91 (0.47—1.76)		1.11 (0.57—2.13)		1.12 (0.57—2.19)	
Keratinization (absent = 1)		0.977		0.680		0.243		0.161
present	1.01 (0.57—1.80)		1.13 (0.64—2.00)		1.41 (0.79—2.54)		1.51 (0.85—2.70)	
Tumor budding (low = 1)		0.173		**0.042**		0.731		0.484
	1.60 (0.81—3.15)		2.03 (1.02—4.05)		0.88 (0.43—1.80)		1.28 (0.63—2.60)	
Cell nest size (large = 1)		0.624		0.135		0.441		0.970
small	1.17 (0.63—2.15)		1.60 (0.86—2.98)		0.77 (0.41—1.46)		1.01 (0.54—1.89)	
Mitoses (low = 1)		**0.009**		0.279		0.050		0.060
high	0.43 (0.23—0.82)		0.72 (0.40—1.30)		0.53 (0.28—1.01)		0.56 (0.30—1.04)	
Nuclear size (small = 1)		**0.038**		0.070		0.916		0.285
large	2.04 (1.02—4.10)		1.81 (0.94—3.47)		1.04 (0.53—2.05)		1.42 (0.75—2.70)	
Stroma content (low = 1)		0.239		0.534		0.536		0.647
high	0.69 (0.38—1.28)		0.83 (0.45—1.50)		1.21 (0.66—2.25)		0.87 (0.47—1.61)	
Necrosis (low = 1)		0.608		0.413		0.712		0.277
high	0.86 (0.48—1.54)		0.79 (0.44—1.40)		0.89 (0.50—1.59)		0.72 (0.40—1.30)	
Inflammation (high = 1)		0.505		0.566		0.525		0.862
low	0.81 (0.43—1.52)		0.83 (0.45—1.55)		0.82 (0.44—1.54)		0.94 (0.50—1.76)	
Lymphovascular invasion (absent = 1)		0.476		0.571		0.065		0.449
present	0.73 (0.31—1.74)		1.25 (0.58—2.71)		0.47 (0.21—1.06)		0.75 (0.35—1.57)	
Perineural invasion (absent = 1)		0.767		0.674		0.431		0.682
present	0.83 (0.25—2.75)		1.28 (0.40—4.17)		1.61 (0.49—5.35)		1.27 (0.39—4.12)	

Funding

This work was supported by the Bundesministerium für Bildung und Forschung (BMBF) e:Med Demonstrators (grant to U.L. 031A426) and by the SeneSys demonstrator (031L0189C).

KK received funding from the DKTK young investigator award.

MB received funding from the Deutsche Krebshilfe (German Cancer Aid) and Else Kröner Fresenius Stiftung.

CRediT authorship contribution statement

Fabian Stögbauer: Conceptualization, Data curation, Formal analysis, Investigation, Methodology, Validation, Visualization, Writing – original draft, Writing – review & editing. **Raik Otto:** Conceptualization, Data curation, Formal analysis, Investigation, Methodology, Software, Validation, Visualization, Writing – original draft, Writing – review & editing. **Korinna Jöhrens:** Data curation, Investigation, Writing – review & editing. **Ingeborg Tinhofer:** Data curation, Supervision, Writing – review & editing. **Ulrich Keilholz:** Supervision, Writing – review & editing. **Christopher Poremba:** Supervision. **Ulrich Keller:** Supervision, Writing – review & editing. **Ulf Leser:** Software, Writing – review & editing. **Wilko Weichert:** Software, Supervision, Writing – review & editing. **Melanie Boxberg:** . **Konrad Klinghammer:** .

Declaration of competing interest

The authors declare that they have no known competing financial interests or personal relationships that could have appeared to influence the work reported in this paper.

Acknowledgements

We thank Victoria Münzer, Hedwig Lammert and Michael Hummel for support in conducting the NanoString analysis, the Institute of Pathology of the Charité and the team of the Core facility "Comparative Experimental Pathology" of the School of Medicine and Health of TUM for excellent technical support. **We acknowledge financial support from the Open Access Publication Fund of Charité – Universitätsmedizin Berlin.**

Appendix A. Supplementary material

Supplementary data to this article can be found online at https://doi.org/10.1016/j.oraloncology.2023.106678.

References

[1] Kaidar-Person O, Gil Z, Billan S. Precision medicine in head and neck cancer. Drug Resist Updat 2018;40:13–6. https://doi.org/10.1016/j.drup.2018.09.001.

[2] Chang J-H, Wu C-C, Yuan K-S-P, Wu ATH, Wu S-Y. Locoregionally recurrent head and neck squamous cell carcinoma: incidence, survival, prognostic factors, and treatment outcomes. Oncotarget 2017;8:55600–12.

[3] Guigay J, Sâada-Bouzid E, Peyrade F, Michel C. Approach to the Patient with Recurrent/Metastatic Disease. Curr Treat Options Oncol 2019;20:65.

[4] Taberna M, Oliva M, Mesía R. Cetuximab-Containing Combinations in Locally Advanced and Recurrent or Metastatic Head and Neck Squamous Cell Carcinoma. Front Oncol 2019;9:383.

[5] Klinghammer K, Gauler T, Dietz A, Grünwald V, Stöhlmacher J, Knipping S, et al. Cetuximab, fluorouracil and cisplatin with or without docetaxel for patients with recurrent and/or metastatic squamous cell carcinoma of the head and neck (CeFCiD): an open-label phase II randomised trial (AIO/IAG-KHT trial 1108). Eur J Cancer 2019;122:53–60. https://doi.org/10.1016/j.ejca.2019.08.018.

[6] Klinghammer K, Otto R, Raguse J-D, Albers AE, Tinhofer I, Fichtner I, et al. Basal subtype is predictive for response to cetuximab treatment in patient-derived xenografts of squamous cell head and neck cancer. Int J Cancer 2017;141:1215–21.

[7] Haddad RI, Seiwert TY, Chow LQM, Gupta S, Weiss J, Gluck I, et al. Influence of tumor mutational burden, inflammatory gene expression profile, and PD-L1 expression on response to pembrolizumab in head and neck squamous cell carcinoma. J Immunother Cancer 2022;10:e003026.

[8] Wang H-C, Yeh T-J, Chan L-P, Hsu C-M, Cho S-F. Exploration of Feasible Immune Biomarkers for Immune Checkpoint Inhibitors in Head and Neck Squamous Cell Carcinoma Treatment in Real World Clinical Practice. Int J Mol Sci 2020;21. https://doi.org/10.3390/ijms21207621.

[9] Walter V, Yin X, Wilkerson MD, Cabanski CR, Zhao N, Du Y, et al. Molecular subtypes in head and neck cancer exhibit distinct patterns of chromosomal gain and loss of canonical cancer genes. PLoS One 2013;8:e56823.

[10] Network CGA. Comprehensive genomic characterization of head and neck squamous cell carcinomas. Nature 2015;517:576–82.

[11] Chen R, Huang Y, Wang L, Zhou J, Tan Y, Peng C, et al. Cetuximab functionalization strategy for combining active targeting and antimigration capacities of a hybrid composite nanoplatform applied to deliver 5-fluorouracil: toward colorectal cancer treatment. Biomater Sci 2021;9:2279–94.

[12] Gomes INF, da Silva-Oliveira RJ, da Silva LS, Martinho O, Evangelista AF, van Helvoort LA, et al. Comprehensive Molecular Landscape of Cetuximab Resistance in Head and Neck Cancer Cell Lines. Cells 2022;11. https://doi.org/10.3390/cells11010154.

[13] Job S, de Reyniès A, Heller B, Weiss A, Guérin E, Macabre C, et al. Preferential Response of Basal-Like Head and Neck Squamous Cell Carcinoma Cell Lines to EGFR-Targeted Therapy Depending on EREG-Driven Oncogenic Addiction. Cancers 2019;11. https://doi.org/10.3390/cancers11060795.

[14] Warren S, Danaher P, Mashadi-Hossein A, Skewis L, Wallden B, Ferree S, et al. Development of Gene Expression-Based Biomarkers on the nCounter Platform for Immuno-Oncology Applications. Methods Mol Biol 2020;2055:273–300.

[15] Veldman-Jones MH, Brant R, Rooney C, Geh C, Emery H, Harbron CG, et al. Evaluating Robustness and Sensitivity of the NanoString Technologies nCounter Platform to Enable Multiplexed Gene Expression Analysis of Clinical Samples. Cancer Res 2015;75:2587–93.

[16] Weichert W, Kossakowski C, Harms A, Schirmacher P, Muley T, Dienemann H, et al. Proposal of a prognostically relevant grading scheme for pulmonary squamous cell carcinoma. Eur Respir J 2016;47:938–46.

[17] Boxberg M, Jesinghaus M, Dorfner C, Mogler C, Drecoll E, Warth A, et al. Tumour budding activity and cell nest size determine patient outcome in oral squamous cell carcinoma: proposal for an adjusted grading system. Histopathology 2017;70:1125–37. https://doi.org/10.1111/his.13173.

[18] Richards CH, Roxburgh CSD, Anderson JH, McKee RF, Foulis AK, Horgan PG, et al. Prognostic value of tumour necrosis and host inflammatory responses in colorectal cancer. Br J Surg 2012;99:287–94.

[19] Ribbat-Idel J, Perner S, Kuppler P, Klapper L, Krupar R, Watermann C, et al. Immunologic "Cold" Squamous Cell Carcinomas of the Head and Neck Are Associated With an Unfavorable Prognosis. Frontiers in Medicine 2021;8. https://doi.org/10.3389/fmed.2021.622330.

[20] Almangush A, Alabi RO, Troiano G, Coletta RD, Salo T, Pirinen M, et al. Clinical significance of tumor-stroma ratio in head and neck cancer: a systematic review and meta-analysis. BMC Cancer 2021;21:480.

[21] Xie S, Liu Y, Qiao X, Hua R-X, Wang K, Shan X-F, et al. What is the Prognostic Significance of Ki-67 Positivity in Oral Squamous Cell Carcinoma? J Cancer 2016;7:758–67.

[22] Brandwein-Gensler M, Teixeira MS, Lewis CM, Lee B, Rolnitzky L, Hille JJ, et al. Oral squamous cell carcinoma: histologic risk assessment, but not margin status, is strongly predictive of local disease-free and overall survival. Am J Surg Pathol 2005;29:167–78.

[23] Dawson H, Lugli A. Molecular and pathogenetic aspects of tumor budding in colorectal cancer. Front Med 2015;2:11.

[24] Lugli A, Zlobec I, Berger MD, Kirsch R, Nagtegaal ID. Tumour budding in solid cancers. Nat Rev Clin Oncol 2021;18:101–15.

[25] Mäkitie AA, Almangush A, Rodrigo JP, Ferlito A, Leivo I. Hallmarks of cancer: Tumor budding as a sign of invasion and metastasis in head and neck cancer. Head Neck 2019;41:3712–8.

[26] Grigore AD, Jolly MK, Jia D, Farach-Carson MC, Levine H. Tumor Budding: The Name is EMT. Partial EMT. J Clin Med Res 2016;5. https://doi.org/10.3390/jcm5050051.

[27] Jesinghaus M, Herz A-L, Kohlruss M, Silva M, Grass A, Lange S, et al. Post-neoadjuvant assessment of tumour budding according to ITBCC subgroups delivers stage- and regression-grade independent prognostic information in intestinal-type gastric adenocarcinoma. Hip Int 2022;8:448–57.

[28] El-Naggar AK, Chan JKC, Grandis JR, Takata T, Slootweg PJ. WHO Classification of Head and Neck Tumours. International Agency for Research on. Cancer 2017.

[29] Budczies J, Klauschen F, Sinn BV, Győrffy B, Schmitt WD, Darb-Esfahani S, et al. Cutoff Finder: a comprehensive and straightforward Web application enabling rapid biomarker cutoff optimization. PLoS One 2012;7:e51862.

[30] Talla SB, Rempel E, Endris V, Jenzer M, Allgäuer M, Schwab C, et al. Immuno-oncology gene expression profiling of formalin-fixed and paraffin-embedded clear cell renal cell carcinoma: Performance comparison of the NanoString nCounter technology with targeted RNA sequencing. Genes Chromosomes Cancer 2020;59:406–16.

[31] Keck MK, Zuo Z, Khattri A, Stricker TP, Brown CD, Imanguli M, et al. Integrative analysis of head and neck cancer identifies two biologically distinct HPV and three non-HPV subtypes. Clin Cancer Res 2015;21:870–81.

[32] Waggott D, Chu K, Yin S, Wouters BG, Liu F-F, Boutros PC. NanoStringNorm: an extensible R package for the pre-processing of NanoString mRNA and miRNA data. Bioinformatics 2012;28:1546–8.

[33] Wickham H. ggplot2: Elegant Graphics for Data Analysis. Springer; 2016.

[34] Website n.d. Wickham H (2022). stringr: Simple, Consistent Wrappers for Common String Operations. http://stringr.tidyverse.org, https://github.com/tidyverse/stringr.

[35] Ritchie ME, Phipson B, Wu D, Hu Y, Law CW, Shi W, et al. limma powers differential expression analyses for RNA-sequencing and microarray studies. Nucleic Acids Res 2015;43:e47.

[36] Phipson B, Lee S, Majewski IJ, Alexander WS, Smyth GK. Robust hyperparameter estimation protects against hypervariable genes and improves power to detect differential expression. Ann Appl Stat 2016:10. https://doi.org/10.1214/16-aoas920.

[37] Website n.d. R Core Team. R: A language and environment for statistical computing. Vienna, Austria: R Foundation for Statistical Computing; 2021. https://www.R-project.org/.

[38] Weber P, Künstner A, Hess J, Unger K, Marschner S, Idel C, et al. Therapy-Related Transcriptional Subtypes in Matched Primary and Recurrent Head and Neck Cancer. Clin Cancer Res 2022;28:1038–52.

[39] Mirabile A, Miceli R, Calderone RG, Locati L, Bossi P, Bergamini C, et al. Prognostic factors in recurrent or metastatic squamous cell carcinoma of the head and neck. Head Neck 2019;41:1895–902.

[40] Kim S-A, Park H, Kim K-J, Kim J-W, Sung JH, Nam M, et al. Amphiregulin can predict treatment resistance to palliative first-line cetuximab plus FOLFIRI chemotherapy in patients with RAS wild-type metastatic colorectal cancer. Sci Rep 2021;11:23803.

[41] Kogashiwa Y, Inoue H, Kuba K, Araki R, Yasuda M, Nakahira M, et al. Prognostic role of epiregulin/amphiregulin expression in recurrent/metastatic head and neck cancer treated with cetuximab. Head Neck 2018;40:2424–31.

[42] Khambata-Ford S, Garrett CR, Meropol NJ, Basik M, Harbison CT, Wu S, et al. Expression of epiregulin and amphiregulin and K-ras mutation status predict disease control in metastatic colorectal cancer patients treated with cetuximab. J Clin Oncol 2007;25:3230–7.

[43] Bai S, Zhang P, Zhang J-C, Shen J, Xiang X, Yan Y-B, et al. A gene signature associated with prognosis and immune processes in head and neck squamous cell carcinoma. Head Neck 2019;41:2581–90.

[44] Patil S, Tawk B, Grosser M, Lohaus F, Gudziol V, Kemper M, et al. Analyses of molecular subtypes and their association to mechanisms of radioresistance in patients with HPV-negative HNSCC treated by postoperative radiochemotherapy. Radiother Oncol 2022;167:300–7. https://doi.org/10.1016/j.radonc.2021.12.049.

[45] Togni L, Caponio VCA, Zerman N, Troiano G, Zhurakivska K, Lo Muzio L, et al. The Emerging Impact of Tumor Budding in Oral Squamous Cell Carcinoma: Main Issues and Clinical Relevance of a New Prognostic Marker. Cancers 2022:14. https://doi.org/10.3390/cancers14153571.

[46] Bossi P, Alfieri S, Strojan P, Takes RP, López F, Mäkitie A, et al. Prognostic and predictive factors in recurrent and/or metastatic head and neck squamous cell carcinoma: A review of the literature. Crit Rev Oncol Hematol 2019;137:84–91.

[47] Maffeis V, Nicolè L, Cappellesso R. RAS, Cellular Plasticity, and Tumor Budding in Colorectal Cancer. Front Oncol 2019;9:1255.

[48] Boxberg M, Leising L, Steiger K, Jesinghaus M, Alkhamas A, Mielke M, et al. Composition and Clinical Impact of the Immunologic Tumor Microenvironment in Oral Squamous Cell Carcinoma. J Immunol 2019;202:278–91.

[49] Almangush A, Salo T, Hagström J, Leivo I. Tumour budding in head and neck squamous cell carcinoma - a systematic review. Histopathology 2014;65:587–94.

[50] Joshi P, Pol J, Chougule M, Jadhav K, Patil S, Patil S. Tumor budding - A promising prognostic histopathological parameter in oral squamous cell carcinoma - A comparative immunohistochemical study. J Oral Maxillofac Pathol 2020;24:587.

[51] Wang H-C, Chan L-P, Cho S-F. Targeting the Immune Microenvironment in the Treatment of Head and Neck Squamous Cell Carcinoma. Front Oncol 2019;9:1084.